



# Graphite/Li<sub>2</sub>ZrO<sub>3</sub> anode for a LiFePO<sub>4</sub> battery

Viona Natalia<sup>1</sup> · Fitria Rahmawati<sup>1,3</sup> · Arinta Wulandari<sup>1</sup> · Agus Purwanto<sup>2,3</sup>

Received: 25 May 2018 / Accepted: 30 October 2018 / Published online: 7 November 2018  
© Institute of Chemistry, Slovak Academy of Sciences 2018

## Abstract

Lithium zirconate, Li<sub>2</sub>ZrO<sub>3</sub> (LZO), was added to graphite anode at various compositions of 0%, 20%, and 30% of weight, and used in a LiFePO<sub>4</sub> (LFP) battery fabrication. The battery cells were designated as LFP//G, LFP//20LZOG, and LFP//30LZOG, respectively. Herein, battery performance was tested to understand LZO contribution to the LFP cathode at different current rates. The data taken were specific capacity of battery, anodic current density, and a crystallite volume change after 50 cycles of charge–discharge. The result found that addition of 20% weight LZO to graphite increases discharge specific capacity after 50 cycles from 71.87 to 72.53 mAhg<sup>-1</sup> with Coulombic efficiency of 99.73%. The capacity retention is 62.1%, which is higher than LFP//G, i.e., 57.7%. The anodic current density of LFP//20LZOG is  $9.09 \times 10^{-6}$  Acm<sup>-2</sup>, also higher than the current density of LFP//G, i.e.,  $8.91 \times 10^{-8}$  Acm<sup>-2</sup>. It indicates contribution of LZO to increase electrochemical reaction rate during battery usage. Structural investigation shows that the LZO addition decreases the volume change of anode material after 50 cycles of charge–discharge under 1C current rate. It indicates that Li<sub>2</sub>ZrO<sub>3</sub> has good structural stability.

**Keywords** Electrochemical property · LiFePO<sub>4</sub> battery · Lithium ion battery (LIB) · Li<sub>2</sub>ZrO<sub>3</sub> · Specific capacity

## Introduction

Clean energy can be divided into three components i.e., harvest, energy storage and conversion of renewable energy such as wind and solar energy (Nitta et al. 2015; Roy and Srivastava 2015). The lithium ion battery (LIBs) is a promising rechargeable battery due to a high-performance charge and discharge, and has a high power density (Braun et al. 2012; Quartarone et al. 2016). Moreover, the introduction of LiFePO<sub>4</sub> (LFP) as cathode material becomes an important advancement, as LIB with LFP cathode is more stable and safe (Padhi et al. 1997). The discharge/charge curves of LFP exhibit a voltage plateau at 3.5 (V) which is independent of the electrode State-Of-Charge (SOC). This behavior

occurs because of the two-phase mechanism inside the LFP particles (Padhi et al. 1997; Yamada et al. 2001; Srinivasan and Newman 2014).

However, long-term operation can cause degradation due to the increasing internal resistance and fading capacity (Bernstein et al. 2012). The growth of solid electrolyte interphase (SEI) layer (Vetter et al. 2005) and lithium plating (Tippmann et al. 2014; Legrand et al. 2014) at the negative electrode or anode are considered as factors to cause loss of capacity and increase of internal resistance (Weißhar and Bessler 2017). Anode material is widely used in a lithium ion battery, i.e., alloying materials (e.g. Sn, Si, Al, Zn), conversion electrode (e.g., oxides, nitrides) and the insertion/extraction type like graphite (Eftekhari 2017; Reddy et al. 2013). The negative electrode that is mostly used in LIB is graphite due to its high abundance and also high theoretical specific capacity of 372 mAhg<sup>-1</sup>, and also low cost (Goriparti et al. 2014; Wenelska et al. 2016). However, graphite also has weakness as it also occurs in a low-potential anode material such as on IVA group elements that have poor cycle ability due to large volume expansion after charge and discharge processes (Kim et al. 2010). The weaknesses are safety issues of dendritic lithium growth produced by its low potential (only about 0.2 V vs Li<sup>+</sup>/Li), and also kinetics

✉ Fitria Rahmawati  
fitria@mipa.uns.ac.id

<sup>1</sup> Research Group of Solid State Chemistry and Catalysis, Chemistry Department, Sebelas Maret University, Jl.Ir. Sutami 36 A Kentingan, Surakarta 57126, Indonesia

<sup>2</sup> Department of Chemical Engineering, Sebelas Maret University, Jl.Ir. Sutami 36 A Kentingan, Surakarta 57126, Indonesia

<sup>3</sup> National Centre for Sustainable Transportation Technology, Institut Teknologi Bandung, Jl. Ganesha 10, Bandung 40132, Indonesia

problems for fast charge–discharge due to solid electrolyte interphase (SEI) layer on graphite surface (Dong et al. 2015).

There are some efforts to overcome the problems, such as by combining graphite with metals, metal oxide, and polymer coating (Wu et al. 2003).  $\text{Li}_2\text{ZrO}_3$  (LZO) may be a promising way to overcome the large volume expansion of graphite. It is known that LZO has been used as anode material (Dong et al. 2015; Li et al. 2009; Zhang et al. 2016) with unit volume change at only  $\sim 0.3\%$  after charge/discharge process (Dong et al. 2015). LZO also shows an excellent cycle performance and rate capability (Dong et al. 2015), and thermodynamically stable against Li (Helstrom and Van Gool 1981). Monoclinic  $\text{Li}_2\text{ZrO}_3$  is an isomorphous of  $\text{Li}_2\text{TiO}_3$  which is known as a good  $\text{Li}^+$  conductor, and thermodynamically stable against Li (Ni et al. 2008; Thackeray et al. 2012).  $\text{Li}_2\text{ZrO}_3$  that was prepared by solid-state reaction shows an excellent cycle performance and rate capability due to its structural stability and high lithium diffusion coefficient, i.e.,  $3.165 \times 10^{-6} \text{ cm}^2 \text{ s}^{-1}$  during reduction, and  $1.919 \times 10^{-6} \text{ cm}^2 \text{ s}^{-1}$  (Ni et al. 2008; Thackeray et al. 2012) during oxidation process. The value is higher than  $\text{Li}_4\text{Ti}_5\text{O}_{12}$ . The theoretical capacity of LZO is  $348 \text{ mAhg}^{-1}$  when  $2\text{Li}^+$  is inserted during charging and released during discharging (Dong et al. 2015). However, substituting graphite anode with LZO may increase production cost, especially for mass production. Therefore, combining LZO properties that provide low volume change after charge/discharge, a highly reversible Li insertion/extraction process, with graphite that has economic advantages may become an interesting solution. A small amount LZO was added to graphite anode, and followed by LFP battery fabrication. The battery performance was tested to understand the LZO contribution of discharge specific capacity ( $\text{mAhg}^{-1}$ ), current density of electrochemical reaction, Coulombic efficiency, capacity retention (%), and also crystalline volume change after 50 cycles. The charge–discharge was conducted under  $0.1 \text{ }^\circ\text{C}$ ,  $0.3 \text{ }^\circ\text{C}$ ,  $0.5 \text{ }^\circ\text{C}$ ,  $0.8 \text{ }^\circ\text{C}$ , and  $1 \text{ }^\circ\text{C}$  to understand its performance whether under low or high current drawn. It may open the way to investigate fast charging battery.

## Experimental

### Preparation of $\text{Li}_2\text{ZrO}_3$

Lithium zirconate was synthesized through solid-state reaction by mixing  $\text{ZrO}_2$  powder (65.21%, produced by caustic fusion of  $\text{ZrSiO}_4$ ) with  $\text{Li}_2\text{CO}_3$  powder (Merck) at a weight ratio of  $\text{ZrO}_2\text{:Li}_2\text{CO}_3 = 1\text{:}1.075$ . This research used self-prepared  $\text{ZrO}_2$  from Indonesian local zircon sand with the specific characteristic published in our previous paper (Rahmawati et al. 2014). An analytical balance (Sartorius, max 110 g, readability 0.001 g) weighed precisely and the

mixture was ground in a ball mill (a homemade, density of the zircon ball is  $4.63 \text{ g/mL}$ , 1 g of mixture was ground by 30 g zirconia balls). The milling was conducted for 2 h at 300 rpm rate, and then continued for next 2 h with 480 rpm rate. The mixture was then heated in a furnace (Kejia Furnace KJ-1700X) at  $950 \text{ }^\circ\text{C}$  for 10 h. The produced lithium zirconate was analyzed with X-ray diffraction instrument (Rigaku miniFlex 600) equipped with Le Bail refinement (RIETICA software) to study its structure and cell parameters. Study on LZO crystal structure has been published in our previous paper (Natalia et al. 2018).

### Electrochemical measurement

The cathode LFP slurry was prepared by mixing LFP powder (90.2 wt%) with PVDF (3.7 wt%), Actylene Black (1.5 wt%), KS-6 (4.6 wt%) and N-Methyl-2-pyrrolidone was used as a solvent. Then, the slurry was coated on aluminum foil with a thickness of  $250 \text{ }\mu\text{m}$  and dried overnight in a vacuum oven at  $120 \text{ }^\circ\text{C}$ . Meanwhile, anode materials used were graphite powder, and the mixture of MCMB (Meso Carbon Micro Beads) and LZO (graphite–LZO) at ratio of 20:80; and 30:70 in accordance with LZO–graphite ratio. The mixture of active material was conducted for 1 h in a high-energy ball milling (Ball Mill MSK-SFM-3) with zirconia balls as crusher. The anode powder (94.5 wt%) was mixed with acetylene black as conductive additive (1.00 wt%), carboxymethyl cellulose (2.25 wt%) and styrene butadiene rubber as a binder (2.25 wt%), and distilled water was used as solvent. The homogeneous paste was then coated on a copper paper at  $100\text{-}\mu\text{m}$  thickness with a doctor blade (MSK-AFA-II), and was dried in a vacuum oven at  $120 \text{ }^\circ\text{C}$  for 24 h and subsequently pressed. The cathode mass was  $30.71 \text{ mg/cm}^2$  and the anode mass was  $14.83 \text{ mg/cm}^2$ . In this prepared battery cell, anode was the limiting electrode and it was used as the basis weight of calculation (Choi et al. 2010). The electrolyte was 1 M  $\text{LiPF}_6$  in EC/DMC (1:1, v:v) and a polypropylene membrane was used as separator. The anode and cathode electrode are rolled with a separator using winding machine type MSK-112A. Then, electrolyte filling is done in an argon-filled glove box. The battery codes referring to the composition are listed in Table 1.

The batteries were charged–discharged between 2.5 and 3.65 V at low current rates of 0.1C, 0.3C, 0.5C, 0.8C and high current rate at 1C for 50 cycles. A 1C of LIBs with graphite anode is  $372 \text{ mAhg}^{-1}$ , and 1C of LIBs with LZO anode is  $348 \text{ mAhg}^{-1}$ . The charge and discharge capacities were recorded in a unit of mAh. Meanwhile, the specific capacity ( $\text{mAhg}^{-1}$ ) was calculated by dividing the capacity (mAh) by the entire mass of anode. The cyclic voltammetry (CV) tests were performed on a CorrTest cs150 electrochemical work station. The voltage range was 0.1–2.5 V and scanning rate was  $1 \text{ mVs}^{-1}$ . CV test of batteries was

**Table 1** The battery code in accordance with LZO content in the anode mixture

Battery code	LZO content (wt%)
LFP//G	0
LFP//10LZOG	10
LFP//20LZOG	20
LFP//30LZOG	30

conducted to analyze electrochemical reaction during charging and discharging processes by applying anode as working electrode, cathode as counter electrode and standard calomel electrode as reference. Meanwhile, CV tests of MCMB and LZO electrode were conducted in a three-neck flask equipped with three electrodes under argon gas. The working electrode (WE) was MCMB/Cu foil or LZO/Cu foil with geometric of 1.5 cm × 1.5 cm. The counter electrode (CE) was lithium metal foil, and the reference electrode (RE) was also lithium metal. The potential interval was 0.1–2.5 V (vs. Li/Li<sup>+</sup>) with scan rate of 1 mVs<sup>-1</sup>.

Impedance measurement was conducted by LCR meter (EUCOL U2826) on those three batteries by applying 0.2 V in the frequency range of 20 Hz–250 kHz. Surface area of the active electrode was 4 cm<sup>2</sup>; meanwhile, the thickness of electrolyte membrane was 25 μm. The impedance data were fitted with ZView software embedded in the instrument, by applying a specific R–C network.

In order to investigate the structural reversibility of LZO upon ion Li<sup>+</sup> intercalation/de-intercalation, the battery disassemble using pliers in glove box, and take the anode to be analyzed its crystal structure with Rigaku MiniFlex 600 X-ray diffraction instrument equipped with Le Bail refinement.

## Result and discussion

### The crystal structure of Li<sub>2</sub>ZrO<sub>3</sub>

The synthesized ZrO<sub>2</sub> is known to have similar diffraction with standard diffraction of ICSD#66787 as it was found in the previous result (Rahmawati et al. 2014). The crystal structure is tetragonal with a space group of *P42/NMCZ*. The synthesized ZrO<sub>2</sub> was then mixed with Li<sub>2</sub>CO<sub>3</sub> to form a Li<sub>2</sub>ZrO<sub>3</sub> by releasing CO<sub>2</sub> during heat treatment at 950 °C for 10 h. A white powder was found with its X-ray diffraction pattern as described in Fig. 1a. The diffraction pattern was then compared with standard diffraction of Li<sub>2</sub>ZrO<sub>3</sub> ICSD#94895, and it proceeds well when the crystal structure, space group, and the cell parameters of the ICSD#94895 were submitted for Le Bail refinement. The Le Bail plot is depicted in Fig. 1b. Le Bail refinement shows that the lithium zirconate was crystallized in a monoclinic phase with a space group of *C12/c1* and the cell parameters, as well as the residual factors, are listed in Table 2. This result is in agreement with LZO that was produced by another researcher (Dong et al. 2015) and in our previous research, with characteristic peaks of Li<sub>2</sub>ZrO<sub>3</sub> at 2θ 20.130°, 26.459° and 39.743° (Natalia et al. 2018).

Surface morphology of the prepared Li<sub>2</sub>ZrO<sub>3</sub> is depicted in Fig. 2. The images show a heterogeneous form and size which is ranging from 1.10 to 2.10 μm as it is also found by our previous research (Natalia et al. 2018). Meanwhile, the commercial MCMB was procured from MTI Corp. with specification as follows: the surface area is 2.022 m<sup>2</sup> g<sup>-1</sup>, particle size is ranging from 1.259 to 52.481 μm, and carbon content is 99.96% (MTI Corporation 2015).

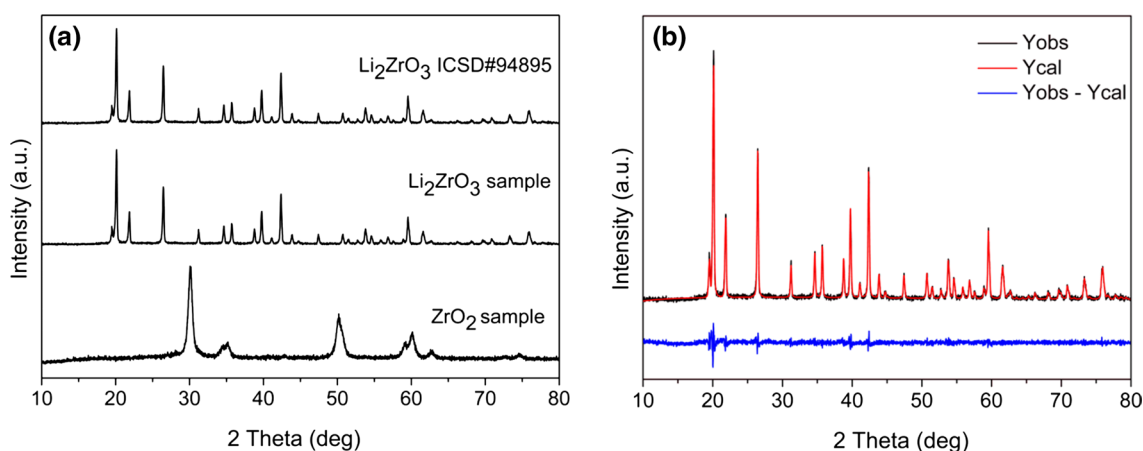


**Fig. 1** **a** The diffraction pattern of the synthesized Li<sub>2</sub>ZrO<sub>3</sub> in comparison with standard diffraction of Li<sub>2</sub>ZrO<sub>3</sub> ICSD#94895, and **b** the Le Bail plot of the prepared Li<sub>2</sub>ZrO<sub>3</sub>

**Table 2** The cell parameters as resulted by Le Bail refinement of the synthesized  $\text{Li}_2\text{ZrO}_3$  with monoclinic structure and space group of  $C12/c1$

$\text{Li}_2\text{ZrO}_3$ ICSD#94895	
Crystal structure	Monoclinic
Space group	$C12/c1$
$a$ (Å)	5.4304 (3)
$b$ (Å)	9.0240 (6)
$c$ (Å)	5.4207 (1)
$\alpha = \gamma$ (°)	90
$\beta$ (°)	112.72 (7)
$Z$	4
$V$ (Å <sup>3</sup> )	245.01 (4)
$R_p$ (%)	6.78
$R_{wp}$ (%)	7.17

## Electrochemical analyses

The charge–discharge curves of the LFP//G and LFP//LZOG battery within the potential window between 2.5 and 3.65 V at the different low current rate are depicted in Fig. 3. The relevant electrochemical data are listed in Table 3. Figure 3a

exhibits the initial charge and discharge capacity at 0.1 °C for the prepared LIBs which is larger than the discharge capacity. The difference between a charge and discharge capacity may be attributed to the side reaction during discharging, such as the formation of solid electrolyte interface (SEI) (Dong et al. 2015). The SEI layers are formed onto the electrode surface due to electrolyte decomposition that occurs in between electrolyte and electrode during the first charge process. The presence of SEI on the electrode surface will prevent direct contact between Li and solvent. The SEI film is also covering the surface electrode that causes capacity lost observed in the first discharge (Wang et al. 2001). Figure 3a shows that at a low current rate of 0.1 C, the LFP//G has the highest charging and discharging capacity. It is in agreement with another researcher (Tran et al. 1996) that graphite has very high capacity under low current rate.

Figure 3b shows the specific capacity as a cycle performance at various current rates of 0.1 °C, 0.3 °C, 0.5 °C, and 0.8 °C. It is found that the increase of current rate allows the decreasing of specific capacity. The same result also found when LZO was combined with Li metal cathode at a

**Fig. 2** Scanning electron microscopy of  $\text{Li}_2\text{ZrO}_3$  at a different magnification as shown by the scale

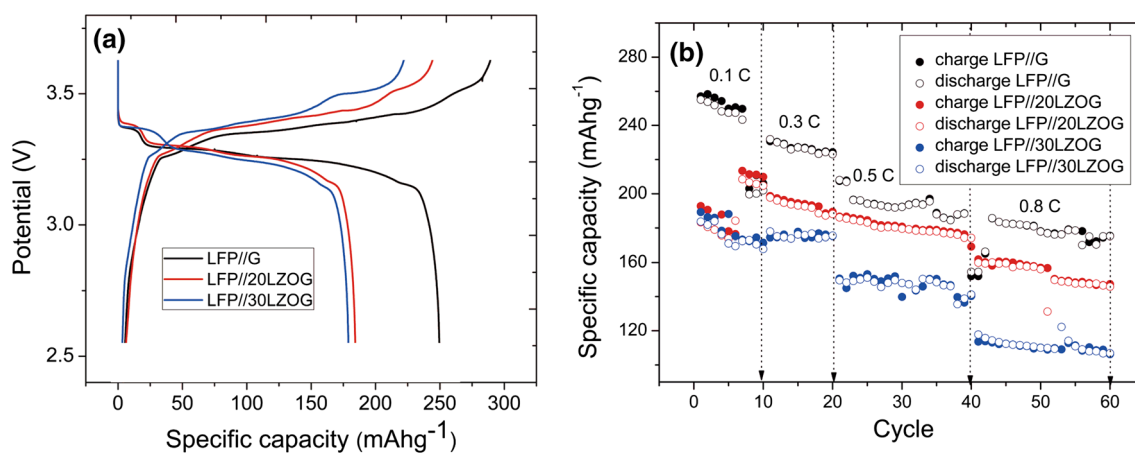
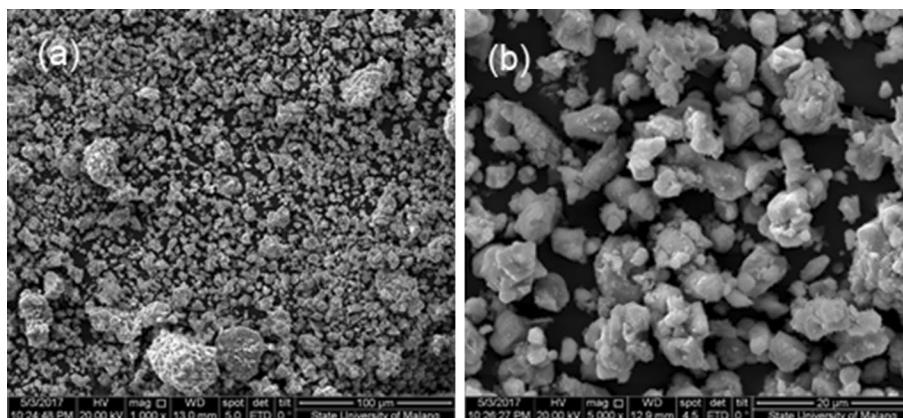


**Fig. 3** a Initial charge and discharge curves of LFP//G and LFP//LZOG under a current rate of 0.1 C and b cycling performance at the different current rate. All test were conducted between 2.5 and 3.65 V at room temperature

**Table 3** Electrochemical data of LFP//G and LFP//LZOG

Sample	Activated at 0.1 °C		Activated at 1 °C			
	Initial discharge capacity (mAhg <sup>-1</sup> )	Initial coulombic efficiency (%)	Initial discharge capacity (mAhg <sup>-1</sup> )	9th discharge capacity (mAhg <sup>-1</sup> )	50th discharge capacity (mAhg <sup>-1</sup> )	Capacity retention after 50 cycles (%)
LFP//G	249.75	86.00	124.56	93.6	71.87	57.7
LFP//20LZOG	184.50	75.15	116.84	102.00	72.53	62.1
LFP//30LZOG	180.20	78.75	85.52	67.45	57.19	66.9

voltage range of 0.1–2.5 V (Dong et al. 2015). A high current rate might cause a rapid volume change that breaks the SEI layer and induces more electrolyte decomposition; thus, more capacity is lost (Wu et al. 2017).

Battery performance test at 1C shows that the LFP//G battery has discharge specific capacity of 124.56 mAhg<sup>-1</sup>, and it decreases significantly to 93.6 mAhg<sup>-1</sup> after 9 cycles. The cycling performance is described in Fig. 4a. It indicates the instability of LFP//G under high current rate. It may be caused by the formation of mossy or dendrite due to the accumulation of Li metal on graphite surface during the intercalation or insertion of Li<sup>+</sup> into the anode crystal lattice at a high current rate (Roušar et al. 1977). This caused the low graphite potential (~0.1 V vs Li/Li<sup>+</sup>) (Eftekhari 2017). The reaction of lithium (dendrite) and electrolyte causes a gas evolution which further increases the cell volume expansion of up to 10%. This volume expansion can induce mechanical stress on the layers of graphite (Birkenmaier et al. 2015). Meanwhile, the LFP//20LZOG battery results discharge specific capacity on the initial and 9th cycle are 116.84 mAhg<sup>-1</sup> and 102 mAhg<sup>-1</sup>, respectively. It indicates that the presence of Li<sub>2</sub>ZrO<sub>3</sub> increases the stability of the battery after charge–discharge under high current. Therefore, even LFP//20LZOG shows a lower initial charge capacity than the LFP//G, i.e., 116.84 mAhg<sup>-1</sup> for LFP//20LZOG and 124.56 mAhg<sup>-1</sup> for LFP//G. However, the LFP//20LZOG

shows a higher capacity retention after 50 cycles than the LFP//G as listed in Table 3. Figure 4a shows that after 50 cycles the charge and discharge capacity of LFP//20LZOG are higher than the LFP//G, and the Coulombic efficiency is high as 99.73%. It is almost 100% as it can be seen in Fig. 4b that the charge and discharge curve is piled up. It indicates a highly reversible Li intercalation/de-intercalation process (Dong et al. 2015) because of the coulombic efficiency or Faraday efficiency.

A significant decrease of the LFP//G specific capacity after cycling at 0.1 °C and just before taking the second cycling at 0.3 °C, as shown in Fig. 3b, indicates that the first 10 cycles are crucial for LFP//G battery especially to reconstruct the atom inside the electrode material after intercalation/de-intercalation. It also happened when a high current rate, 1C, is drawn from the battery as it is described in Fig. 4a at the first 10 cycles. The large decrease of the specific capacity after the first 10 cycles, as well as a sudden increase of the specific capacity after the second 10 cycles may be caused by a loss of electrical contact between anode/cathode and the current collector (Krause et al. 2016); then, it was stopped for the first round, and started for the next round with a different current rate.

During charging–discharging process, lithium ions were inserted and extracted from its crystal host, Li<sub>2</sub>ZrO<sub>3</sub>, as it is described in Eq. (1) (Dong et al. 2015). Meanwhile,

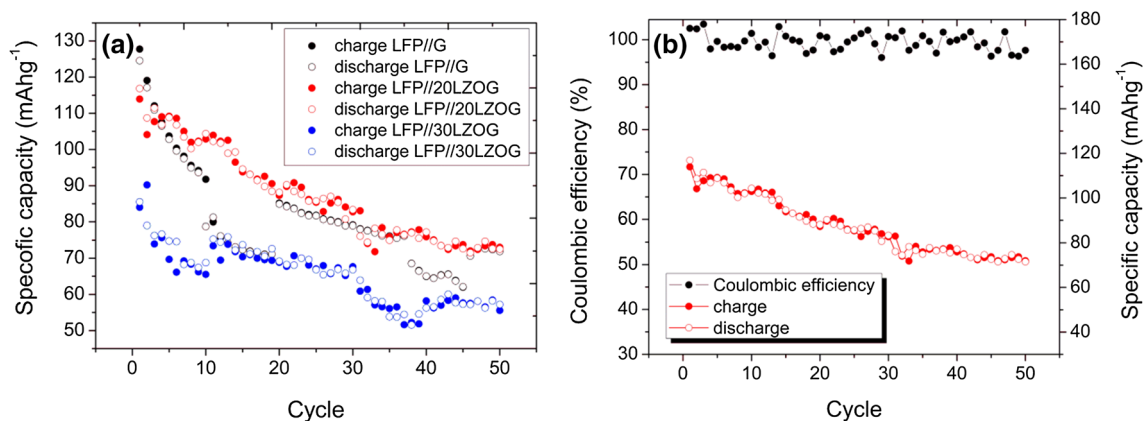
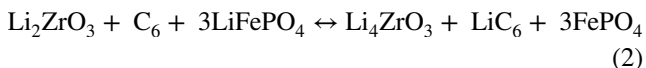
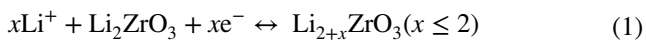


**Fig. 4** a Cycling performance of LFP//G and LFP//LZOG battery and b the coulombic efficiency and capacity retention of the LFP//20LZOG. All test were conducted at the high current rate at 1 C between 2.5 and 3.65 V at room temperature

prediction of the reaction using LFP//LZOG battery is as in the Eq. (2).



The potential of lithiated carbon is close to that of Li metal, i.e., 0.0–0.5 V (Linden and Reddy 2002). On comparing with other researchers on LZO application for LIBs, it

was found that this LFP//20LZOG is in a high initial capacity of  $184.5 \text{ mAh.g}^{-1}$ , a high potential of 3.2–3.4 V and an intermediate specific current rate of  $0.037 \text{ Ag}^{-1}$ , as listed in Table 4.

The plot of  $\log i$  vs.  $E$  of LFP//20LZOG and LFP//0LZOG is depicted in Fig. 5. Higher current density represents higher oxidation–reduction reaction rate, as confirmed by the relation between reaction and current density (Eq. 3). The high current density also refers to the high current produced by the battery (Roušar et al. 1977)

**Table 4** The potential for a definite specific capacity. The specific capacities are reported by some references

Material	Applications	Counter electrode	Initial capacity ( $\text{mAh.g}^{-1}$ )	Potential (V)	Current rate ( $\text{Ag}^{-1}$ )	References
$\text{Li}_2\text{ZrO}_3$	Anode	Li metal	160	0.1–1.7	0.029	Dong et al. (2015)
$\text{Li}_2\text{ZrO}_3$ coated $\text{Li}_4\text{Ti}_5\text{O}_{12}$	Anode	Li metal	168	1.4–1.8	0.016	Zhang et al. (2016)
$\text{Li}_2\text{ZrO}_3$ -encapsulated $\text{LiNi}_{0.5}\text{Co}_{0.2}\text{MnO}_2$	Cathode	Li metal	117	3.5–3.9	1.5	Wu et al. (2015)
$\text{Li}_2\text{ZrO}_3$ -encapsulated $\text{LiNi}_{0.5}\text{Co}_{0.2}\text{MnO}_2$	Cathode	Graphite	140	3.5–3.9	0.15	Wu et al. (2015)
$\text{Li}_2\text{ZrO}_3$ coated Si/graphite/C	Anode	Li metal	215	0.25–0.6	0.168	Li et al. (2009)
$\text{Li}_2\text{ZrO}_3$ /graphite	Anode	$\text{LiFePO}_4$	184.5	3.2–3.4	0.037	This research

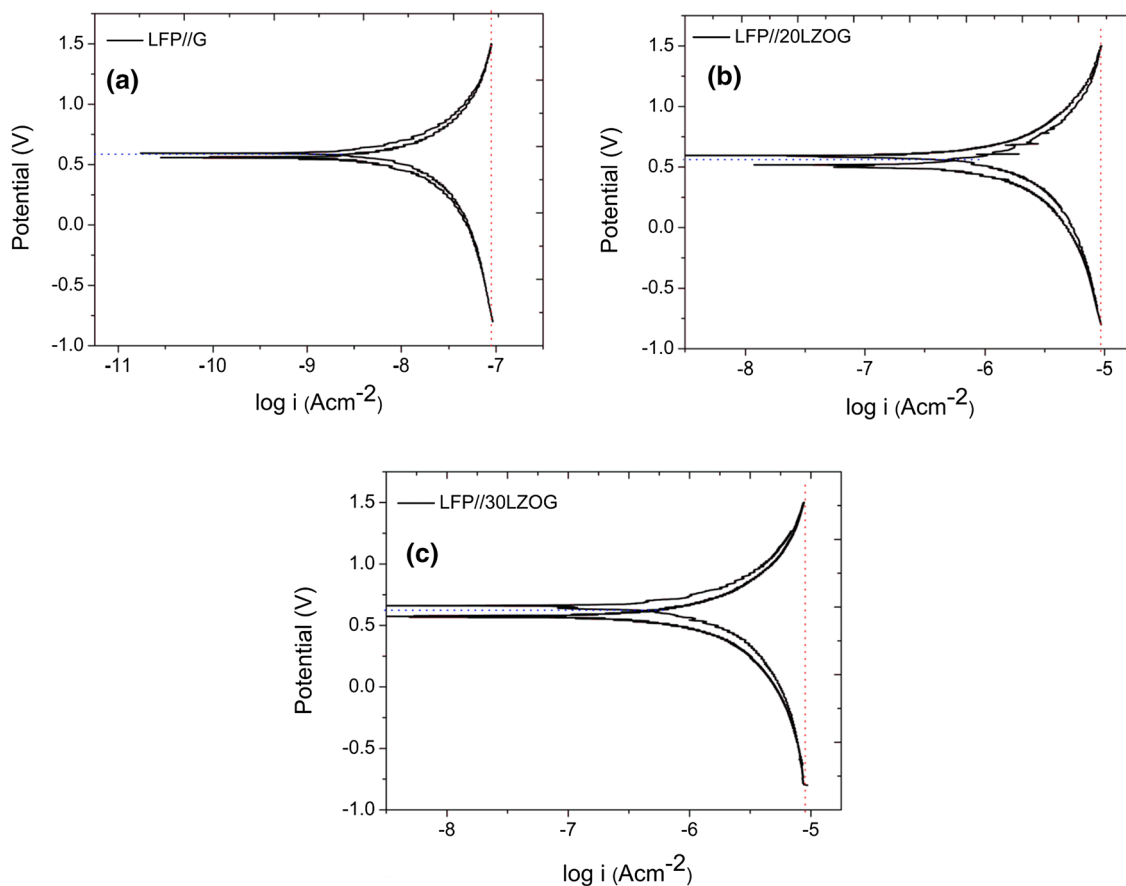


**Fig. 5** Plots of potential (V) to  $\log i$  ( $\text{mAcm}^{-2}$ ) of LFP//G, LFP//20LZOG and LFP//0LZOG at sweeping rate of  $1 \text{ mVs}^{-1}$

due to a high reaction rate provided by the battery. The relation between current density ( $\text{mAcm}^{-2}$ ) and the reaction rate is described in Eq. (3).

$$r = i/nF, \tag{3}$$

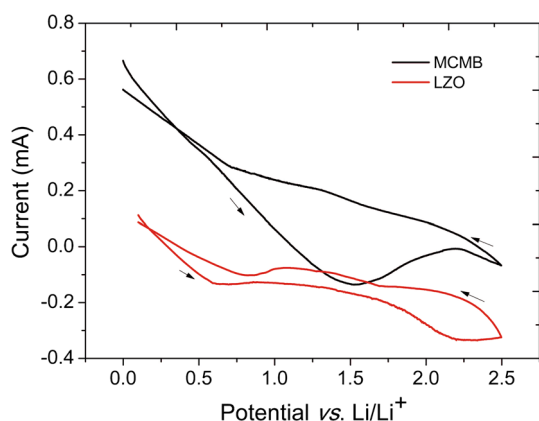
where  $r$  is the total reaction rate, a function of anodic reaction and cathodic reaction,  $i$  is the current density ( $\text{A cm}^{-2}$ ), and  $F$  is the Faradaic number. The LFP//20LZOG and LFP//30LZOG show a higher current density than LFP//G. The values are  $9.09 \times 10^{-6} \text{ Acm}^{-2}$  and  $8.97 \times 10^{-6} \text{ Acm}^{-2}$ . Meanwhile, the current density of LFP//G is  $8.91 \times 10^{-8} \text{ Acm}^{-2}$ . All three batteries show a similar anodic and cathodic current density as described

in Fig. 5. It indicates that the batteries were not polarized and have a similar oxidation–reduction rate promising a high durability.

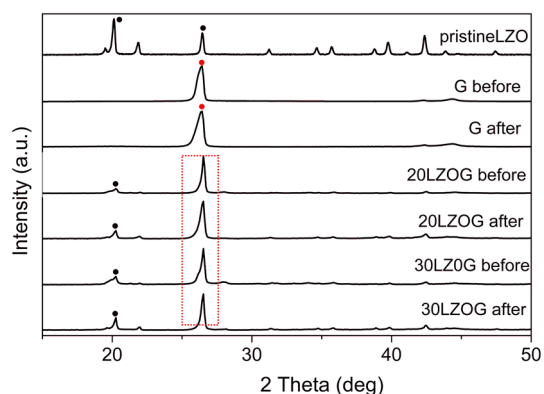
Cyclic voltammetry, CV, of MCMB and LZO electrode with a potential scan between 0.0 and 2.5 V is shown in

**Table 5** Resistance of the prepared batteries as resulted from impedance data fitting with the specific R–C network as described in Fig. 7

Anode	$R_s$ ( $\Omega$ )	$R_p$ ( $\Omega$ )	Resistance ( $\Omega$ )
10LZOG	– 9600.00	65190	74790.00
20LZOG	98.84	2364	2265.16
30LZOG	519.8	6126	5606.20

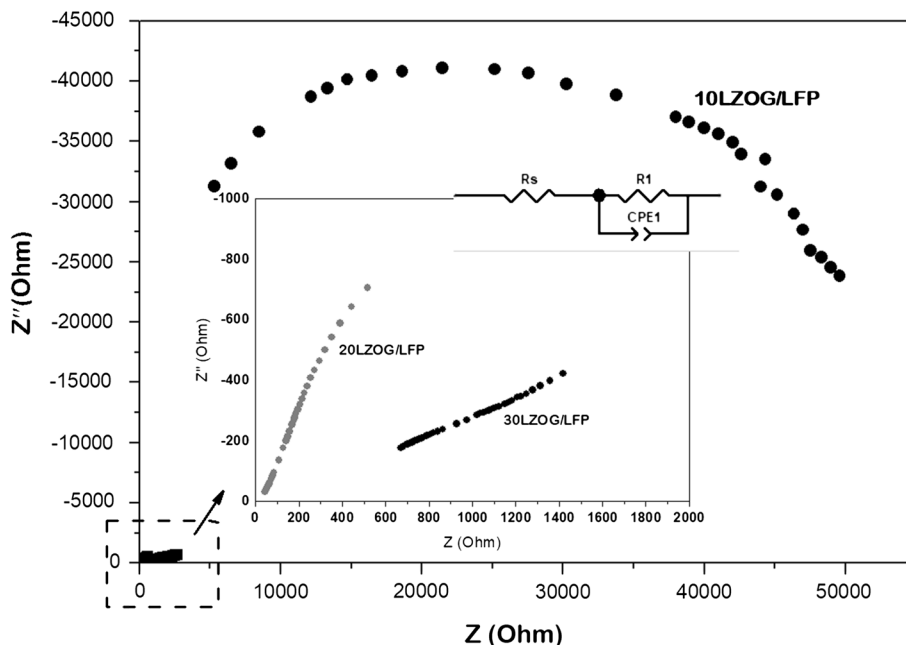


**Fig. 6** Cyclic voltammetry curve of MCMB and LZO electrode with potential range of 0.0–2.5 V in 1 M  $\text{LiPF}_6/\text{EC}:\text{DMC}$  (1:1). Scan rate 1 mV/s



**Fig. 8** The evolution of the XRD pattern of the anode electrode before and after the intercalation/de-intercalation lithium process after 50 cycles. (●: monoclinic  $\text{Li}_2\text{ZrO}_3$ , ●: graphite)

**Fig. 7** Impedance plot of 10LZOG/LFP, 20LZOG/LFP, and 30LZOG/LFP with the R–C network model for fitting



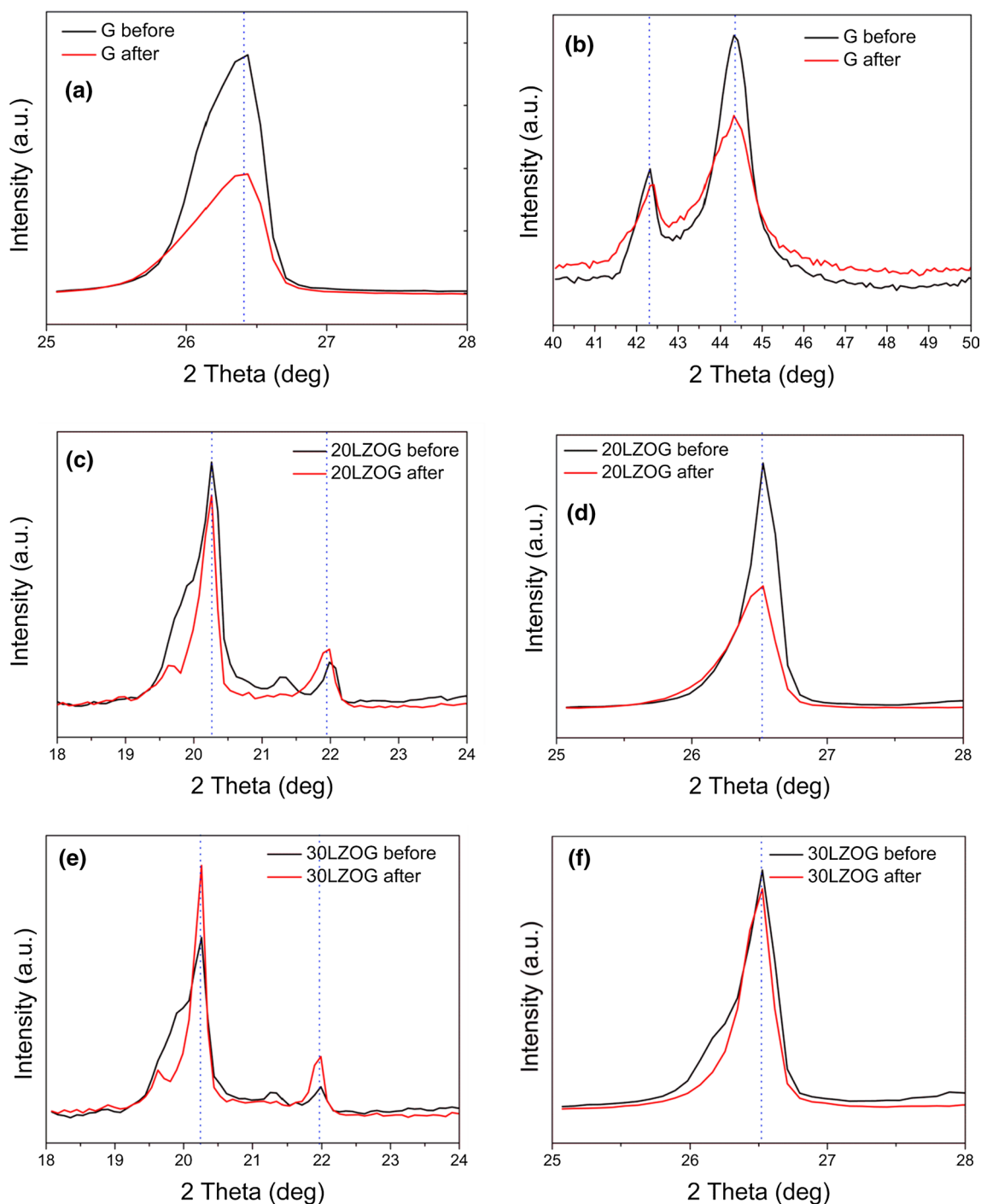


**Fig. 9** The zoom on the select regions of the XRD pattern of the anode electrode before and after the intercalation/de-intercalation lithium process after 50 cycles

**Fig. 6.** The CV curve of MCMB shows the lithiation and delithiation into or from MCMB in the potential range of 0.0–1.5 V (vs.  $\text{Li}/\text{Li}^+$ ) (Zhao et al. 2000). Meanwhile, CV curve of LZO shows reduction peaks at about 0.63 and 2.2 V which indicate the lithiation and the Solid Electrolyte Interface, SEI, formation (Dong et al. 2015). The oxidation peaks

at about 1.08 and 2.02 V can be attributed to the delithiation process (Dong et al. 2015). The CV result shows that LZO addition may increase the active potential of the anode.

The Nyquist plots of the prepared batteries are shown in Fig. 7, along with the R–C network for fitting. A ZView fitting found the resistances as listed in Table 5. It is found



**Table 6** The volume change of graphite, 20LZOG, and 30LZOG obtained from the XRD refinement result before and after the charge–discharge process of 50 cycles

Cell Name	Phase	$V (\text{Å}^3)$		$\Delta V (\text{Å}^3)$	Mean $\Delta V (\text{Å}^3)$
		Before	After		
LFP//G	Graphite	35.83(3)	36.38(6)	0.543	0.543
LFP//20LZOG	$\text{Li}_2\text{ZrO}_3$	247.96(1)	248.23(5)	0.270	0.528
	Graphite	35.82(2)	36.60(3)	0.788	
LFP//30LZOG	$\text{Li}_2\text{ZrO}_3$	248.04(1)	248.10(4)	0.063	0.321
	Graphite	35.80(9)	36.38(9)	0.579	

that the resistance on 10LZOG//LFP is very high, 74.79 k $\Omega$ . It is 33 times higher than 20LZOG//LFP, and it is 13.3 times higher than 30LZOG//LFP. The very high resistance has caused the 10LZOG//LFP did not perform during charge–discharge test.

To investigate the structural reversibility of LZO upon Li intercalation/de-intercalation, the XRD analysis was conducted on the anode material after 50 cycles of the charge–discharge process. The results are described in Fig. 8 in comparison with the XRD of the initial anode material. Peaks at  $2\theta$  of 20.26° and 26.52° are the main characteristics of  $\text{Li}_2\text{ZrO}_3$ , while graphite shows a specific peak at  $2\theta$  26.3°. The magnification of each characteristic peaks as shown in Fig. 9 can elaborate a slight change that might occur after 50 cycles. Figure 9a–c show that the  $2\theta$  of characteristic peaks did not change. The changes are mostly on the width of peaks that may correlate with the change of the cell parameters and also indicating that the crystallinity decreases. A Le Bail refinement was conducted to understand the changes in cell parameters, by submitting standard parameters of a hexagonal graphite ICSD#53781 with a space group of  $p63/mmc$ . Meanwhile, the refinement on LZOG was conducted by submitting two phases of a standard hexagonal graphite ICSD#53781 with space group  $p63/mmc$  and a standard monoclinic lithium zirconate ICSD #94895 with a space group of  $C12/c1$ . The results are listed in Table 6. It confirms that the addition of  $\text{Li}_2\text{ZrO}_3$  allows lower volume change after 50 cycles than the volume change when only graphite was used as the anode.

## Conclusion

Lithium zirconate,  $\text{Li}_2\text{ZrO}_3$ , was successfully prepared by solid-state reaction with  $\text{Li}_2\text{CO}_3$  and  $\text{ZrO}_2$  from zircon sand as precursors. The crystal structure of the prepared  $\text{Li}_2\text{ZrO}_3$  is monoclinic with a space group of  $C12/c1$ . The addition of 20% weight of  $\text{Li}_2\text{ZrO}_3$  to the graphite anode could increase the charge–discharge capacity of the LFP battery as well as its specific capacity and its coulombic efficiency at a high current rate of 1C. The presence of  $\text{Li}_2\text{ZrO}_3$  also decreases the anode volume change after 50 cycles of charge–discharge, indicating the stability of the battery even under high

current rate. It is a promising result for fast charging and a durable LIBs battery.

**Acknowledgement** This research is a part of Hibah Mandatory 2017, contract number of 623/UN27.21/PP/2017, Sebelas Maret University, Republic of Indonesia, and a part of USAID Sustainable Higher Education Research Alliances (USAID SHERA) Prime Award No. AID-497-A16-0004, subaward No. IIE00000078-ITB-1. Authors acknowledge the support.

## Compliance with ethical standards

**Conflict of interest** On behalf of all authors, the corresponding author states that there is no conflict of interest.

## References

- Bernstein N, Johannes MD, Hoang K (2012) Origin of the structural phase transition in  $\text{Li}_7\text{La}_3\text{Zr}_2\text{O}_{12}$ . *Phys Rev Lett* 109:205702. <https://doi.org/10.1103/PhysRevLett.109.205702>
- Birkenmaier C, Bitzer B, Harzheim M, Hintennach A, Schleid T (2015) Lithium plating on graphite negative electrodes: innovative qualitative and quantitative investigation methods. *J Electrochem Soc* 162:A2626–A2650. <https://doi.org/10.1149/2.0451514jes>
- Braun PV, Cho J, Pikul JH, King WP, Zhang H (2012) High power rechargeable batteries. *Curr Opin Solid State Mater Sci* 16:186–198. <https://doi.org/10.1016/j.cossms.2012.05.002>
- Choi D, Wang D, Viswanathan VV, Bae I, Wang W, Nie Z, Zhang J, Graff GL, Liu J, Yang Z, Duong T (2010) Electrochemistry communications Li-ion batteries from  $\text{LiFePO}_4$  cathode and anatase/graphene composite anode for stationary energy storage. *Electrochem Commun* 12(3):378–381. <https://doi.org/10.1016/j.elecom.2009.12.039>
- Dong Y, Zhao Y, Duan H, Huang J (2015) Electrochemical performance and lithium-ion insertion/extraction mechanism studies of the novel  $\text{Li}_2\text{ZrO}_3$  anode materials. *Electrochim Acta* 161:219–225. <https://doi.org/10.1016/j.electacta.2015.01.220>
- Eftekhari A (2017) Low voltage anode materials for lithium-ion batteries. *Energy Storage Mater* 7:157–180. <https://doi.org/10.1016/j.ensm.2017.01.009>
- Goriparti S, Miele E, De Angelis F, Di Fabrizio F, Zaccaria RP, Capiglia C (2014) Review on recent progress of nanostructured anode materials for Li-ion batteries. *J Power Sources* 257:421–443. <https://doi.org/10.1016/j.jpowsour.2013.11.103>
- Helstrom W, Van Gool W (1981) Li ion conduction in  $\text{Li}_2\text{ZrO}_3$ ,  $\text{Li}_4\text{ZrO}_4$ , and  $\text{LiScO}_2$ . *Solid State Ionics* 2:59–64. [https://doi.org/10.1016/0167-2738\(81\)90021-7](https://doi.org/10.1016/0167-2738(81)90021-7)
- Kim H, Bak S, Kim K (2010)  $\text{Li}_4\text{Ti}_5\text{O}_{12}$ /reduced graphite oxide nano-hybrid material for high rate lithium-ion batteries.

- Electrochem Commun 12:1768–1771. <https://doi.org/10.1016/j.elecom.2010.10.018>
- Krause A, Dörfler S, Piwko M, Wisser FM, Jaumann T, Ahrens E, Giebeler L, Althues H, Schädlich S, Grothe J, Jeffery A, Grube M, Brückner J, Martin J, Eckert J, Kaskel S, Mikolajick T, Weber WM (2016) High area capacity lithium-sulfur full-cell battery with prelithiated Silicon nanowire-carbon anodes for long cycling stability. *Sci Rep* 6:1–12. <https://doi.org/10.1038/srep27982>
- Legrand N, Knosp B, Desprez P, Lapique F, Raël S (2014) Physical characterization of the charging process of a Li-ion battery and prediction of Li plating by electrochemical modelling. *J Power Sources* 245:208–216. <https://doi.org/10.1016/j.jpowsour.2013.06.130>
- Li M, Qu M, He X, Yu Z (2009) Electrochemical properties of  $\text{Li}_2\text{ZrO}_3$ -coated silicon/graphite/carbon composite as anode material for lithium ion batteries. *J Power Sources* 188:546–551. <https://doi.org/10.1016/j.jpowsour.2008.12.010>
- Linden D, Reddy TB (2002) Handbook of batteries, 3d ed. McGraw-Hill Library of Congress Cataloging-in-Publication Data
- MTI Corporation (2015). Specification and safety data sheet MCMB
- Natalia V, Rahmawati F, Purwanto A (2018) Crystal structure analysis of lithium zirconate prepared from local sand at a various ratio of  $\text{Li}_2\text{CO}_3$  to  $\text{ZrO}_2$ . *J Mat Env Sci* 9:1152–1158. <https://doi.org/10.26872/jmes.2018.9.4.126>
- Ni J, Zhou H, Chen J, Zhang X (2008) Improved electrochemical performance of layered  $\text{LiNi}_{0.4}\text{Co}_{0.2}\text{Mn}_{0.4}\text{O}_2$  via  $\text{Li}_2\text{ZrO}_3$  coating. *Electrochim Acta* 53:3075–3083. <https://doi.org/10.1016/j.electacta.2007.11.026>
- Nitta N, Wu F, Lee JT, Yushin G (2015) Li-ion battery materials: present and future. *Mater Today* 18(5):252–264. <https://doi.org/10.1016/j.mattod.2014.10.040>
- Padhi AK, Nanjundaswamy KS, Goodenough JB (1997) Phosphoolivines as positive-electrode materials for rechargeable lithium batteries. *J Electrochem Soc* 144:1188–1194. <https://doi.org/10.1149/1.1837571>
- Quartarone E, Dall'Asta V, Resmini A, Tealdi C, Tredici IG, Tamburini UA, Mustarelli P (2016) Graphite-coated ZnO nanosheets as high-capacity, highly stable, and binder-free anodes for lithium-ion batteries. *J Power Sources* 320:314–321. <https://doi.org/10.1016/j.jpowsour.2016.04.107>
- Rahmawati F, Permadani I, Soepriyanto S, Syarif D, Herald E (2014) Double steps leaching and filtration in caustic fusion method to produce zirconia from local zircon concentrate. *Icopia*. <https://doi.org/10.2991/icopia-14.2015.18>
- Reddy MV, Subba Rao GV, Chowdari BVR (2013) Metal oxides and oxysalts as anode materials for Li ion batteries. *Chem Rev* 113:5364–5457. <https://doi.org/10.1021/cr3001884>
- Roušar Cezner V, Neješpová J, Jackšić MM, Spasojević M, Nikolić BZ (1977) Calculation of local current densities and terminal voltage for a monopolar sandwich electrolyser: application to chlorate cells. *J Appl Electrochem* 7:427–435. <https://doi.org/10.1007/BF00615947>
- Roy P, Srivastava SK (2015) Nanostructured anode materials for lithium ion batteries. *J Mater Chem A* 3(6):2454–2484. <https://doi.org/10.1039/C4TA04980B>
- Srinivasan V, Newman J (2014) Discharge model for the lithium iron-phosphate electrode. *J Electrochem Soc* 151:A1517–A1529. <https://doi.org/10.1149/1.1785012>
- Thackeray M, Wolverton C, Isaacs ED (2012) Electrical energy storage for transportation—approaching the limits of, and going beyond, lithium-ion batteries. *Energy Environ Sci* 5:7854–7863. <https://doi.org/10.1039/C2EE21892E>
- Tippmann S, Walper D, Balboa L, Spier B, Bessler WF (2014) Low-temperature charging of lithium-ion cells part I: electrochemical modeling and experimental investigation of degradation behavior. *J Power Sources* 252:305–316. <https://doi.org/10.1016/j.jpowsour.2013.12.022>
- Tran TD, Feikert JH, Pekala RW, Kinoshita K (1996) Rate effect on lithium-ion graphite electrode performance. *J Appl Electrochem* 26:1161–1167. <https://doi.org/10.1007/BF00243741>
- Vetter J, Novák P, Wagner MR, Veit C (2005) Ageing mechanisms in lithium-ion batteries. *J Power Sources* 147:269–281. <https://doi.org/10.1016/j.jpowsour.2005.01.006>
- Wang C, Appleby AJ, Little FE (2001) Charge-discharge stability of graphite anodes for lithium-ion batteries. *J Electroanal Chem* 497:33–46. [https://doi.org/10.1016/S0022-0728\(00\)00447-2](https://doi.org/10.1016/S0022-0728(00)00447-2)
- Weißhar B, Bessler WG (2017) Model-based lifetime prediction of an LFP/graphite lithium-ion battery in a stationary photovoltaic battery system. *J Energy Storage* 14:179–191. <https://doi.org/10.1016/j.est.2017.10.002>
- Wenelska K, Ottmann A, Schneider P, Thauer E, Klingeler R, Mijowska E (2016) Hollow carbon sphere/metal oxide nanocomposites anodes for lithium-ion batteries. *Energy* 103:100–106. <https://doi.org/10.1016/j.energy.2016.02.063>
- Wu YP, Rahm E, Holze R (2003) Carbon anode materials for lithium ion batteries. *J Power Sources* 114:228–236. [https://doi.org/10.1016/S0278-7753\(02\)00596-7](https://doi.org/10.1016/S0278-7753(02)00596-7)
- Wu H, Wang Z, Liu S, Zhang L, Zhang Y (2015) Fabrication of  $\text{Li}^+$ -conductive  $\text{Li}_2\text{ZrO}_3$ -based shell encapsulated  $\text{LiNi}_{0.5}\text{Co}_{0.2}\text{Mn}_{0.3}\text{O}_2$  microspheres as high-rate and long-life cathode materials for Li-ion batteries. *ChemElectroChem* 2:1921–1928. <https://doi.org/10.1002/celec.201500303>
- Wu Y, Keil P, Schuster SF, Jossen A (2017) Impact of temperature and discharge rate on the aging of a  $\text{LiCoO}_2/\text{LiNi}_{0.8}\text{Co}_{0.15}\text{Al}_{0.05}\text{O}_2$  lithium-ion pouch cell. *J Electrochem Soc* 164:A1438–A1445. <https://doi.org/10.1149/2.0401707jes>
- Yamada A, Kudo Y, Liu K (2001) Phase Diagram of  $\text{Li}_x(\text{Mn}_y\text{Fe}_{1-y})\text{PO}_4$  ( $0 \leq x, \leq y \leq 1$ ). *J Electrochem Soc* 148:A1153–A1158. <https://doi.org/10.1149/1.1401083>
- Zhang H, Liu Y, Wang T, Yang Y, Shi S, Yang G (2016)  $\text{Li}_2\text{ZrO}_3$ -coated  $\text{Li}_4\text{Ti}_5\text{O}_{12}$  with nanoscale interface for high performance lithium-ion batteries. *Appl Surf Sci* 368:56–62. <https://doi.org/10.1016/j.apsusc.2016.01.244>
- Zhao M, Kariuku S, Dewald HD, Lemke FR, Staniewicz RJ, Plichta EJ, Marsh RA (2000) Electrochemical stability of copper in lithium-ion battery electrolytes. *J Electrochem Soc* 147(8):2874–2879. <https://doi.org/10.1149/1.1393619>